


Differentiation of Intrahepatic Cholangiocarcinoma and Hepatic Lymphoma Based on Radiomics and Machine Learning in Contrast-Enhanced Computer Tomography

Technology in Cancer Research & Treatment
Volume 20: 1-7
© The Author(s) 2021
Article reuse guidelines:
sagepub.com/journals-permissions
DOI: 10.1177/15330338211039125
journals.sagepub.com/home/tct


Hanyue Xu, MD^{1,2,*}, Xiuhe Zou, PhD^{3,*}, Yunuo Zhao, MD^{1,2},
Tao Zhang, MD^{1,2}, Youyin Tang, MD⁴, Aiping Zheng, MD^{1,2},
Xianghong Zhou, MD^{1,2}, and Xuelei Ma, PhD¹ 

Abstract

Purpose: This study aimed to explore the ability of texture parameters combining with machine learning methods in distinguishing intrahepatic cholangiocarcinoma (ICCA) and hepatic lymphoma (HL). **Method:** A total of 28 patients with HL and 101 patients with ICCA were included. A total of 45 texture features were extracted by the software LifeX from contrast-enhanced computer tomography (CECT) images and 38 of them were eligible. A total of 5 feature selection methods and 9 feature classification methods were used to build the best diagnostic models, combining with the 10-fold cross-validation to assess the accuracy of these models. The discriminative ability of each model was evaluated by receiver operating characteristic analysis. **Result:** A total of 45 predictive models were built by the cross combination of each selection and classification method to differentiate ICCA from HL. According to the results of test group, most of the models performed well with a large area under the curve (AUC) (>0.85) and high accuracy (>0.85). Random Forest (RF)_Linear Discriminant Analysis (LDA) (AUC = 0.997, accuracy = 0.969) was the best model among all the 45 models. **Conclusion:** Combining texture parameters from CECT with multiple machine learning models can differentiate ICCA and HL effectively, and RF_LDA performed the best in this process.

Keywords

intrahepatic cholangiocarcinoma, hepatic lymphoma, contrast-enhanced computer tomography, texture, machine learning

Abbreviations

Adaboost, Adaptiveboosting; AI, artificial intelligence; AUC, area under the curve; CECT, contrast-enhanced computer tomography; DC, distance correlation; DT, decision tree; GaussianNB, Gaussian Naïve Bayes; HL, hepatic lymphoma; GBDT, gradient boosted decision tree; ICCA, intrahepatic cholangiocarcinoma; KNN, k-nearest neighbor; LASSO, least absolute shrinkage and selection operator; LDA, linear discriminant analysis; LR, logistic regression; PHL, primary hepatic lymphoma; RF, random forest; ROI, regions-of-interest; SHL, secondary hepatic lymphoma; SVM, support vector machine; XGBoost, eXtreme gradient boosting.

Received: April 19, 2021; Revised: June 30, 2021; Accepted: July 22, 2021.

¹ Department of Biotherapy, West China Hospital, Sichuan University, Chengdu 610041, PR China

² West China School of Medicine, West China Hospital, Sichuan University, Chengdu 610041, PR China

³ Department of Thyroid Surgery, West China Hospital of Sichuan University, Chengdu 610041, PR China

⁴ Department of Liver surgery, West China Hospital, Sichuan University, Chengdu 610041, PR China

*Hanyue Xu and Xiuhe Zou contributed equally to the article.

Corresponding Author:

Xuelei Ma, Department of Biotherapy, West China Hospital, Sichuan University, No. 37, Guoxue Alley, Chengdu 610041, PR China.

Email: drmaxuelei@gmail.com



Creative Commons Non Commercial CC BY-NC: This article is distributed under the terms of the Creative Commons Attribution-NonCommercial 4.0 License (<https://creativecommons.org/licenses/by-nc/4.0/>) which permits non-commercial use, reproduction and distribution of the work without further permission provided the original work is attributed as specified on the SAGE and Open Access page (<https://us.sagepub.com/en-us/nam/open-access-at-sage>).

Introduction

Intrahepatic cholangiocarcinoma (ICCA) is the second most common primary malignancy in liver.¹ Though the primary hepatic lymphoma (PHL) is rare, secondary hepatic lymphoma (SHL) is quite common and counts for 20% of non-Hodgkin lymphoma.² The treatments of these 2 diseases are different: surgery is the only method to cure ICCA, while chemotherapy plays important role in treating HL.³ Thus, accurate differentiation of these 2 diseases in the early stage is necessary for choosing appropriate treatment.

Traditional radiological diagnosis is not objective enough, as the number of traditional image features is limited, and the interpretation of these results depends on the experience of radiologists to some extent. Meanwhile, with the development of radiological techniques, like

contrast-enhanced computer tomography (CECT), magnetic resonance imaging, and contrast-enhanced ultrasound, more digital parameters can be obtained, enabling quantitative radiological diagnosis.^{4,5} To promote objective diagnosis, digital and artificial intelligence (AI) methods are developed prosperously in recent years.

Texture parameter is related to digital image information, which cannot be seen by naked eyes, describing the heterogeneity of the regions-of-interest (ROI).⁶ Previous studies have used texture analysis and AI in the diagnosis, staging, treatment plan, and prognosis prediction of hepatic diseases.⁷ For instance, texture analysis and topological data with 3 machine learning (ML) models were used in classifying different malignant liver masses.⁸ The differentiation of ICCA and HL has not been studied in the AI area and the

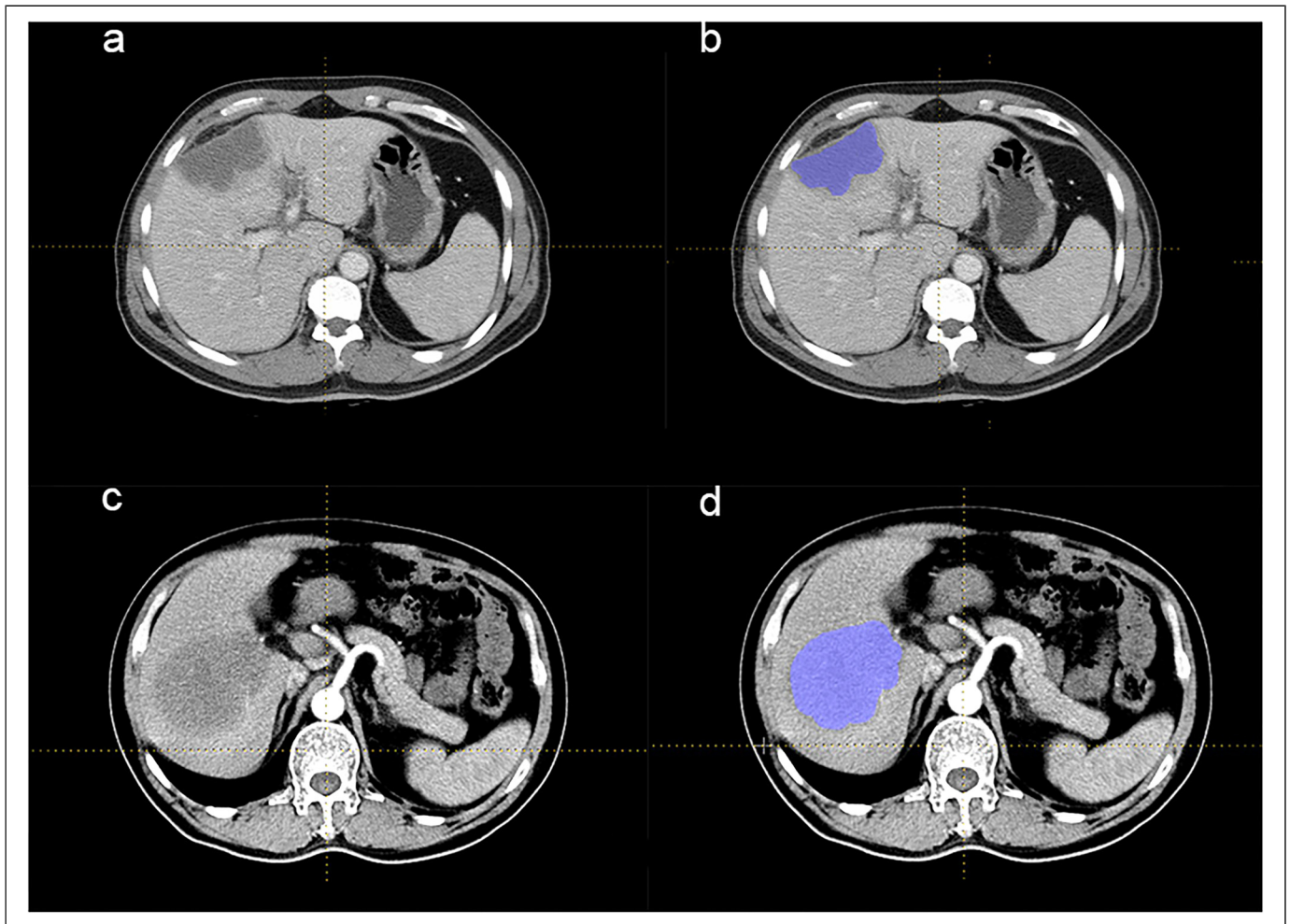


Figure 1. CECT of patients with ICCA and HL. (a and b) The CECT images of 1 ICCA patient. This patient presented with intermittent dull pain in the right upper abdomen with postprandial pain that had been evident for 8 years and worsened for 20 days. No nausea, vomiting, or yellowish skin staining was found. An irregular and mixed low-density mass was seen in the left internal lobe of the liver, with a blurred boundary and a size of about 8.1×3.9 cm on CECT. (c and d) The CECT images of 1 HL patient. This patient was admitted to the hospital for 3 months with intermittent fever, night sweats, and pain in the right chest, accompanied by decreased appetite and no yellowing of the skin. On CECT, a soft tissue mass with slightly lower density was seen in the lower segment of the right lobe of liver, about 8.8×8.7 cm, with an ill-defined boundary and uneven moderate enhancement. The boundary between the lesion and the right anterior and posterior portal vein branches was not clear. ROIs were all drawn along the liver lesion slice by slice, and all areas of calcification and necrosis were excluded.

Abbreviations: ICCA, intrahepatic cholangiocarcinoma; CECT, contrast-enhanced computer tomography; HL, hepatic lymphoma; ROI, region of interest.

discrimination of these 2 diseases needs the combination of clinical, laboratorial, and radiological results in clinical practice. Thus, in this study, we purposed to explore the ability of combining texture analysis with ML to differentiate these 2 malignant liver diseases.

Method

Patient Enrollment

This study was approved by the ethic committee of West China Hospital, Sichuan University and no written informed consent was required. From January 2014 to October 2019, a total of 129 patients from West China Hospital was involved, and all of their diagnoses were confirmed histologically (28 were HL and 101 were ICCA). The inclusion criteria were that patients had: (1) histologically diagnoses of ICCA or HL, (2) full electronic medical record, (3) abdominal contrast CT images. The exclusion criteria were that: (1) patients have incomplete information or low-resolution images, (2) patients have other diseases which can influence the image significantly like liver cirrhosis.

Contrast CT Data Acquisition and ROI Segmentation

All of the CECT images were obtained by Philips Brilliance 64-slice detector-row machines (Philips Healthcare). The enhanced scan (120 kVp, 200 mA, pitch 0.891 to 1.235; collimation 64×0.625 mm) was initiated 30 s (hepatic arterial phase) and 90 s (portal venous phase) after injection of the contrast medium (1.5-2.0 mL/kg, Iohexol: Beijing Beilu Pharmaceutical), using a power injector (Stellant D, Medrad) with the speed of 2 to 3 mL/s.

Texture Feature Extraction

Texture features were extracted by the software LifeX (version 3.74, French Alternative Energies and Atomic Energy Commission), an open-source platform that can analyze and extract plenty of quantitative parameters from digital images.⁹ ROIs on the delayed phase were independently drawn by 2

readers with more than 5 years of clinical experience. All the results were supervised by a third reader with 15-year clinical experience to deal with different opinions. Three-dimensional ROIs were built by the accumulation of all two-dimensional region ROIs, which were delineated around the boundary of lesions in each layer of transaxially CT images. Respective examples of CECT images and ROIs of ICCA and HL patients were shown in Figure 1.

Feature Selection and Classification Methods

In this study, 5 feature selection methods were used, including distance correlation (DC), random forest (RF), least absolute shrinkage and selection operator (LASSO), eXtreme gradient boosting (XGBoost), and gradient boosted decision tree (GBDT) methods. Python software was used to conduct feature selection methods. Meanwhile, 9 feature classification methods were used in feature classification. These classification methods were linear discriminant analysis (LDA), support vector machine (SVM), random forest (RF), Adaptiveboosting (Adaboost), *k*-nearest neighbor (KNN), Gaussian Naïve Bayes (GaussianNB), logistic regression (LR), GBDT, and decision tree (DT). A total of 45 models were built based on the combination of these 5 selection methods and 9 classification methods.

Diagnostic Model Built by ML

The patients were randomly divided into 2 groups, a training group and a test group, in the proportion of 4:1. The algorithms deployment procedure was assessed by 10-fold cross-validation, guaranteeing the maximum use of data and promote the accuracy of models.¹⁰ The sensitivity, specificity, areas under the receiver operating characteristic curve (AUC), and accuracy were calculated to assess the differential ability of the 45 models (Figure 2). To explore the necessary of ML selection methods, the 3 features with the optimal AUC in the single feature joint LDA classification detection were used for modeling. The ML algorithms were all programmed using the Python (version 3.6.4) ML library known as scikit-learn (version 19.0).

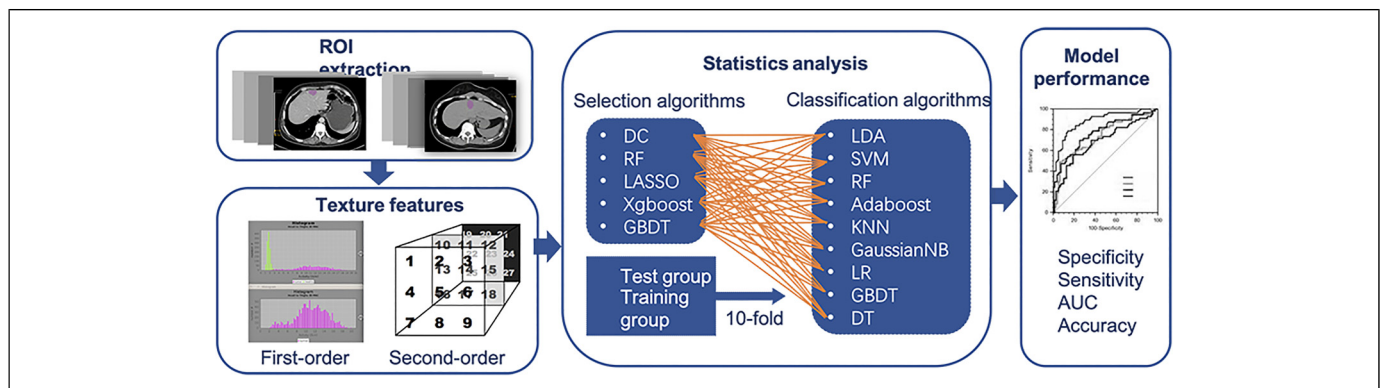


Figure 2. The flowchart of this study.

Abbreviations: AUC, areas under the receiver operating characteristic curve; DC, distance correlation; RF, random forest; LASSO, least absolute shrinkage and selection operator; XGBoost, eXtreme gradient boosting; GBDT, gradient boosted decision tree; LDA, linear discriminant analysis; ROI, region of interest; SVM, support vector machine; Adaboost, Adaptiveboosting; KNN, *k*-nearest neighbor; GaussianNB, Gaussian Naïve Bayes; LR, logistic regression; DT, decision tree.

Table 1. Clinical Parameters of ICCA and HL.

	ICCA (N = 101)	HL (N = 28)	
Age	58.2 ± 10.8	53.2 ± 17.9	
Sex (M: F)	55: 46	17: 11	
Size		NA	
<5 cm	24		
5 to 10 cm	71		
>10 cm	6		
Differentiated degree		NA	
Poorly differentiated	26		
Medium to low differentiated	54		
Medium differentiated	19		
Medium to high differentiated	2		
Stage		PHL (N = 8)	SHL (N = 20)
II	NA	1	1
III		1	
IV			25

Abbreviations: ICCA, intrahepatic cholangiocarcinoma; HL, hepatic lymphoma; M: F male: female; NA, not appropriate; PHL, primary hepatic lymphoma; SHL, secondary hepatic lymphoma.

Results

Characteristics of the Study Cohort

The clinical and pathological characteristics of the ICCA and HL patients were summarized in Table 1. The mean age of ICCA patients was 58.2 (10.8), and that of HL patients was 53.2 (17.9). The gender ratios were 55:46 and 17:11 (male: female) for ICCA and HL patients, respectively. In terms of the pathological findings, there were 26 poorly differentiated, 54 poorly to moderately differentiated, 19 moderately differentiated, and 2 moderately to highly differentiated ICCA patients. Among HL patients included, 8 were PHL and 20 were SHL.

Characteristics of Texture Parameters

A total of 45 features were extracted from the CECT images of each patient and 38 of them were eligible. They included 4 histogram-based matrixes, 3 shape-based matrixes, 6 gray-level co-occurrence matrixes, 11 gray-level run length matrixes, 3 neighborhood gray-level dependence matrixes, and 11 gray-level zone length matrixes (Supplemental Material 1). The definitions of texture parameters were shown in Supplemental Material 2, and the features selected by each selection methods were listed in Supplemental Material 3.

Diagnostic Performance of Models

Features were selected by 5 methods and classified by 9 methods. Thus, a total of 45 predictive models were built by the combination of the feature selection and feature classification methods. We used underline to combine the name of

Table 2. The Differentiation Ability of all Models Based on 5 Feature Selection Methods and 9 Feature Classification Methods.

Models	Test group			
	Sensitivity	Specificity	Accuracy	AUC
OD_LDA	0.990	0.833	0.954	0.953
DC_LDA	0.990	0.867	0.962	0.997
RF_LDA	0.990	0.900	0.969	0.997
LASSO_LDA	0.950	0.500	0.853	0.788
Xgboost_LDA	0.980	0.933	0.969	0.993
GBDT_LDA	0.990	0.867	0.962	0.980
OD_SVM	0.990	0.833	0.923	0.987
DC_SVM	0.990	0.867	0.962	0.993
RF_SVM	1.000	0.900	0.954	0.987
LASSO_SVM	1.000	0.500	0.792	0.915
Xgboost_SVM	0.970	0.933	0.938	0.990
GBDT_SVM	1.000	0.867	0.962	0.983
OD_RF	0.970	0.717	0.915	0.983
DC_RF	0.990	0.833	0.954	0.990
RF_RF	0.980	0.733	0.923	0.990
LASSO_RF	0.980	0.783	0.938	0.958
Xgboost_RF	0.990	0.833	0.954	0.995
GBDT_RF	0.990	0.783	0.946	0.997
OD_Adaboost	0.990	0.767	0.938	0.987
DC_Adaboost	0.961	0.750	0.915	0.962
RF_Adaboost	0.980	0.783	0.938	0.983
LASSO_Adaboost	0.960	0.750	0.915	0.933
Xgboost_Adaboost	0.990	0.800	0.946	0.990
GBDT_Adaboost	0.980	0.900	0.962	0.993
OD_KNN	0.960	0.633	0.884	0.955
DC_KNN	0.960	0.800	0.923	0.970
RF_KNN	0.980	0.767	0.931	0.970
LASSO_KNN	0.970	0.450	0.861	0.912
Xgboost_KNN	0.950	0.783	0.915	0.962
GBDT_KNN	0.980	0.800	0.938	0.977
OD_GaussianNB	0.980	0.767	0.931	0.923
DC_GaussianNB	0.970	0.867	0.946	0.953
RF_GaussianNB	0.910	0.867	0.900	0.935
LASSO_GaussianNB	0.950	0.467	0.846	0.907
Xgboost_GaussianNB	0.950	0.867	0.931	0.950
GBDT_GaussianNB	0.940	0.900	0.931	0.935
OD_LR	0.990	0.583	0.900	0.953
DC_LR	1.000	0.633	0.915	0.957
RF_LR	1.000	0.667	0.923	0.967
LASSO_LR	1.000	0.000	0.783	0.909
Xgboost_LR	1.000	0.400	0.869	0.952
GBDT_LR	1.000	0.483	0.885	0.990
OD_GBDT	0.960	0.783	0.923	0.898
DC_GBDT	0.980	0.850	0.954	0.932
RF_GBDT	0.960	0.783	0.923	0.917
LASSO_GBDT	0.980	0.817	0.946	0.941
Xgboost_GBDT	0.970	0.850	0.946	0.932
GBDT_GBDT	0.980	0.783	0.938	0.937
OD_DT	0.970	0.783	0.931	0.877
DC_DT	0.980	0.750	0.931	0.865
RF_DT	0.970	0.750	0.923	0.860
LASSO_DT	0.960	0.750	0.915	0.855
Xgboost_DT	0.980	0.750	0.931	0.865
GBDT_DT	0.990	0.750	0.938	0.870

Abbreviations: Adaboost, Adaptiveboosting; AUC, area under the curve; DC, distance correlation; DT, decision tree; GaussianNB, Gaussian Naïve Bayes; GBDT, gradient boosted decision tree; ICCA, intrahepatic cholangiocarcinoma; KNN, *k*-nearest neighbor; LASSO, least absolute shrinkage and selection operator; LDA, linear discriminant analysis; LR, logistic regression; RF, random forest; SVM, support vector machine; OD, original data; XGBoost, eXtreme gradient boosting.

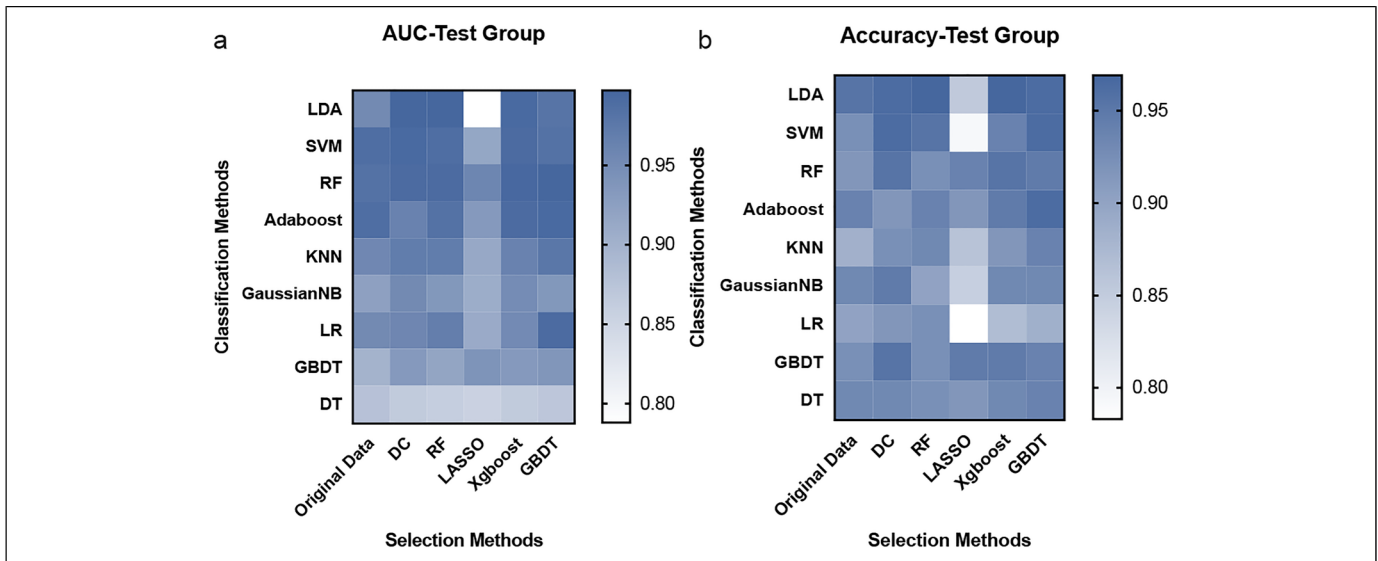


Figure 3. The heatmap of AUC and accuracy of 45 models in the test group.

Abbreviations: AUC, areas under the receiver operating characteristic curve; DC, distance correlation; RF, random forest; LASSO, least absolute shrinkage and selection operator; XGBoost, eXtreme gradient boosting; GBDT, gradient boosted decision tree; LDA, linear discriminant analysis; SVM, support vector machine; Adaboost, Adaptiveboosting; KNN, *k*-nearest neighbor; GaussianNB, Gaussian Naïve Bayes; LR, logistic regression; DT, decision tree.

both selection and classification methods to name the models. The diagnostic ability of each model was listed in Table 2. Models with the highest AUC and accuracy (>0.96) were distance correlation (DC)_linear discriminant analysis (LDA) (0.997, 0.962) and random forest (RF)_LDA (0.997, 0.969) (AUC and accuracy, respectively). Heatmaps of AUC and accuracy of the test group were presented in Figure 3. To figure out the necessity of using ML selection methods, we compared the AUC of each feature and selected the top 3 features to build a model by the LDA classification method. The AUC of this model without ML selection was 0.975 and the accuracy was 0.899 (AUCs of each single feature were in Supplemental Material 4).

Discussion

Early and accurate differentiation of ICCA and HL is necessary for treatment. Meanwhile, image features with much digital information can be explored to facilitate this process. Texture parameters combining with ML promote the imaging diagnosis to be more objective and precise.¹¹ To elevate the radiological diagnosis and enhance its ability in assisting clinical diagnosis, this study used texture parameters and ML to differentiate CCA and HL. The results showed texture parameters can differentiate ICCA from HL effectively as long as choosing suitable ML models.

ICCA and HL have similar features in CECT, low attenuation masses with clear rim,^{12–14} increasing the difficulty of image diagnosis, which can be influenced by the experience of radiologists. The specific diagnosis of these 2 diseases depends on histopathological results by surgical excisional biopsies or computer tomographic/ultrasound transcutaneous biopsies, which are invasive and have selection bias. Though

patients with SHL have systemic symptoms and diffused lesions on images, systemic symptoms also exist in patients with advanced stages ICCA and intrahepatic isolated masses also exist in SHL images.¹⁵ Several studies had reported cases, in which HL mimicked ICCA and multiple modalities were required for diagnosis.^{16–18} For example, a study tried to use serum alkaline phosphatase isoenzyme electrophoresis to differentiate the 2 diseases.¹⁹ To improve the radiological diagnosis capacity, texture analysis combining with ML is the most potential method waiting to be explored.

As the histological differences are the basic of differential diagnosis and some studies have proved that histological features can reflect on digital images.²⁰ Thus, we hypothesize that the differences of components of ICCA and HL can also be uncovered by texture analysis. Texture combining with ML has been used in many precious studies for promoting staging, diagnosis, and therapy response of many diseases.^{21,22} In terms of liver, previous studies used a convolutional neural network to differentiate malignant indeterminate and benign liver masses with an overall accuracy of 0.84.²³ Besides digital images, hematoxylin and eosin-stained whole-slide images can also be analyzed by deep learning methods in differentiating malignant liver masses (AUC >0.85).²⁴ To our knowledge, this is the first study that used multiple ML models and texture features to distinguish ICCA and HL. Meanwhile, compared with previous studies that used only several algorithms in feature selection and classification, our study built 45 models to guarantee that proper parameters can be selected and effective classification methods can be used, as there is not any general model being suitable for all the issues.^{25–28}

In our study, RF_LDA performs the best in differentiating ICCA and HL and followed by RF_LDA. Comparing the

AUC and accuracy of LDA models built with and without ML feature selection, higher diagnostic ability was found in LDA models with ML selection. To some extent, this result indicated the superiority of ML selection. LDA is the simplest classification method with low cost and well performance. It separates parameters by projecting a line and guarantees the discriminative ability by maximizing the ratio of intergroup variance to the intragroup variance.²⁹ RF is an effective method for both feature selection and classification by using the training bootstrap samples to build subtrees and choosing the classification depending on the number of votes. It can deal with not only linear but also nonlinear variables with high accuracy and resistance to overtraining.³⁰ A previous study used ML methods for exploring prognostic biomarkers of advanced nasopharyngeal carcinoma, and found RF_RF with performed the best.³¹

There are some limitations to this study. Firstly, the number of HL enrolled is limited as HL does not have high provenance, and larger cohorts are required in the future study. Secondly, this study is hold in a single hospital, and thus, the generalization performance may be suspected. However, texture parameter extraction and model establishment are conducted by open-source packages, guaranteeing repeatability by other researchers. Moreover, this study only explored texture parameters of CECT, other radiological modalities are supposed to be studied and compared to figure out the most effective radiological method for distinguishing these 2 diseases. In conclusion, combining texture parameters from CECT with multiple ML models can differentiate ICCA and HL effectively, and _LDA performed the best in this process.

Authors' Contributions

HY X, XH Z, and XL M contributed to the study design. AP Z and YY T contributed to the data collection, YN Z, XH Z, and T Z contributed to the data analysis. All authors contributed to the writing or revising of this manuscript. All authors have read and approved this version of manuscript to be published and agree to be responsible for all aspects of the work.

Availability of Data and Materials

The datasets used and/or analyzed during the current study are available from the corresponding author on reasonable request.

Declarations

Ethics approval and consent to participate were obtained from the ethic committee of West China Hospital.


Declaration of Conflicting Interests

The authors declared no potential conflicts of interest with respect to the research, authorship, and/or publication of this article.

Funding

The authors received no financial support for the research, authorship and/or publication of this article.

ORCID iD

Xuelei Ma  <https://orcid.org/0000-0002-9148-5001>

Supplemental Material

Supplemental material for this article is available online.

References

1. Galia M, Taibbi A, Marinetti D, et al. Focal lesions in cirrhotic liver: what else beyond hepatocellular carcinoma? *Diagn Interv Radiol.* 2014;20(3):222-228.
2. Ippolito D, Porta M, Maino C, et al. Diagnostic approach in hepatic lymphoma: radiological imaging findings and literature review. *J Cancer Res Clin Oncol.* 2020;146(6):1545-1558.
3. Blechacz B, Gores GJ. Cholangiocarcinoma: advances in pathogenesis, diagnosis, and treatment. *Hepatology.* 2008;48(1):308-321.
4. Curtis WA, Fraum TJ, An H, et al. Quantitative MRI of diffuse liver disease: current applications and future directions. *Radiology.* 2019;290(1):23-30.
5. Zhai L, Qiu LY, Zu Y, et al. Contrast-enhanced ultrasound for quantitative assessment of portal pressure in canine liver fibrosis. *World J Gastroenterol.* 2015;21(15):4509-4516.
6. Gillies RJ, Kinahan PE, Hricak H. Radiomics: images are more than pictures, they are data. *Radiology.* 2016;278(2):563-577.
7. Lambin P, Leijenaar RTH, Deist TM, et al. Radiomics: the bridge between medical imaging and personalized medicine. *Nat Rev Clin Oncol.* 2017;14(12):749-762.
8. Oyama A, Hiraoka Y, Obayashi I, et al. Hepatic tumor classification using texture and topology analysis of non-contrast-enhanced three-dimensional T1-weighted MR images with a radiomics approach. *Sci Rep.* 2019;9(1):8764.
9. Nioche C, Orhac F, Boughdad S, et al. LIFEx: a freeware for radiomic feature calculation in multimodality imaging to accelerate advances in the characterization of tumor heterogeneity. *Cancer Res.* 2018;78(16):4786-4789.
10. Molinaro AM, Simon R, Pfeiffer RM. Prediction error estimation: a comparison of resampling methods. *Bioinformatics.* 2005; 21(15):3301-3307.
11. Giger ML. Machine learning in medical imaging. *J Am Coll Radiol.* 2018;15(3 Pt B):512-520.
12. Rajesh S, Bansal K, Sureka B, et al. The imaging conundrum of hepatic lymphoma revisited. *Insights Imaging.* 2015;6(6):679-692.
13. Tomasian A, Sandrasegaran K, Elsayes KM, et al. Hematologic malignancies of the liver: spectrum of disease. *Radiographics.* 2015;35(1):71-86.
14. Seo N, Kim DY, Choi JY. Cross-sectional imaging of intrahepatic cholangiocarcinoma: development, growth, spread, and prognosis. *AJR Am J Roentgenol.* 2017;209(2):W64-W75.
15. Bridgewater J, Galle PR, Khan SA, et al. Guidelines for the diagnosis and management of intrahepatic cholangiocarcinoma. *J Hepatol.* 2014;60(6):1268-1289.
16. Forghani F, Masoodi M, Kadivar M. Primary hepatic lymphoma mimicking cholangiocarcinoma. *Oman Med J.* 2017;32(4):335-338.

17. Kawakami H, Kubota Y, Ban T. Primary hepatic diffuse large B-cell lymphoma mimicking intrahepatic cholangiocarcinoma. *Intern Med.* 2019;58(1):143-144.
18. Park JI, Jung BH. Primary hepatic lymphoma treated with liver resection followed by chemotherapy: a case report. *Ann Hepatobiliary Pancreat Surg.* 2017;21(3):163-167.
19. Yasri S, Wiwanitkit V. How to discriminate between primary hepatic lymphoma and cholangiocarcinoma. *Oman Med J.* 2018;33(5):447.
20. Sohn YM, Han K, Seo M. Immunohistochemical subtypes of breast cancer: correlation with clinicopathological and radiological factors. *Iran J Radiol.* 2016;13(4):e31386.
21. Hyun SH, Ahn MS, Koh YW, et al. A machine-learning approach using PET-based radiomics to predict the histological subtypes of lung cancer. *Clin Nucl Med.* 2019;44(12):956-960.
22. Ji GW, Zhu FP, Xu Q, et al. Machine-learning analysis of contrast-enhanced CT radiomics predicts recurrence of hepatocellular carcinoma after resection: a multi-institutional study. *EBioMedicine.* 2019;50(2019):156-165.
23. Yasaka K, Akai H, Abe O, et al. Deep learning with convolutional neural network for differentiation of liver masses at dynamic contrast-enhanced CT: a preliminary study. *Radiology.* 2018;286(3):887-896.
24. Kiani A, Uyumazturk B, Rajpurkar P, et al. Impact of a deep learning assistant on the histopathologic classification of liver cancer. *NPJ Digit Med.* 2020;3(2020):23.
25. Bisdas S, Shen H, Thust S, et al. Texture analysis- and support vector machine-assisted diffusional kurtosis imaging may allow in vivo gliomas grading and IDH-mutation status prediction: a preliminary study. *Sci Rep.* 2018;8(1):6108.
26. Feng Z, Rong P, Cao P, et al. Machine learning-based quantitative texture analysis of CT images of small renal masses: differentiation of angiomyolipoma without visible fat from renal cell carcinoma. *Eur Radiol.* 2018;28(4):1625-1633.
27. Mannil M, von Spiczak J, Manka R, et al. Texture analysis and machine learning for detecting myocardial infarction in noncontrast low-dose computed tomography: unveiling the invisible. *Invest Radiol.* 2018;53(6):338-343.
28. Park YW, Oh J, You SC, et al. Radiomics and machine learning may accurately predict the grade and histological subtype in meningiomas using conventional and diffusion tensor imaging. *Eur Radiol.* 2019;29(8):4068-4076.
29. Lotte F, Bougrain L, Cichocki A, et al. A review of classification algorithms for EEG-based brain-computer interfaces: a 10 year update. *J Neural Eng.* 2018;15(3):031005.
30. van der Ploeg T, Austin PC, Steyerberg EW. Modern modelling techniques are data hungry: a simulation study for predicting dichotomous endpoints. *BMC Med Res Methodol.* 2014;14(2014):137.
31. Zhang B, Tian J, Dong D, et al. Radiomics features of multiparametric MRI as novel prognostic factors in advanced nasopharyngeal carcinoma. *Clin Cancer Res.* 2017;23(15):4259-4269.